UC Santa Barbara

UC Santa Barbara Previously Published Works

Title

A new insight on the core–shell structure of zerovalent iron nanoparticles and its application for Pb(II) sequestration

Permalink

https://escholarship.org/uc/item/7mj986m2

Authors

Zhang, Yalei
Su, Yiming
Zhou, Xuefei
et al.

Publication Date

2013-12-01

DOI

10.1016/j.jhazmat.2013.10.031

Peer reviewed

A new insight on the core–shell structure of zerovalent iron nanoparticles and its application for Pb(II) sequestration

Yalei Zhang [a,b,*], Yiming Su [a], Xuefei Zhou [a,**], Chaomeng Dai [a,c], Arturo A. Keller [d]

[a] State Key Laboratory of Pollution Control and Resources Reuse, Tongji University, Shanghai 200092, China
[b] Key Laboratory of Yangtze Water Environment for Ministry of Education, Tongji University, Shanghai 200092, China
[c] College of Civil Engineering, Tongji University, Shanghai 200092, China
[d] Bren School of Environmental Science & Management, University of California, Santa Barbara, USA

HIGHLIGHTS

- The shell of nZVI is composed of 45.5% $Fe(OH)_3$ and 54.5% FeOOH.
- $Fe(OH)_3$ shell suppresses the reduction of Pb(II).
- $Fe(OH)_3$ shell greatly promotes the co-precipitation and adsorption of Pb(II).
- pH < 4.5 favors Fe dissolution, while pH > 4.5 promotes Pb(II) adsorption.
- A reaction between Fe^0 core, $Fe(OH)_3$ and Pb(II) is proposed.

ARTICLE INFO

ABSTRACT

Nanoscale zerovalent iron (nZVI) has shown a high efficacy for removing heavy metals from liquid solution. However, its removal capacity has not been fully explored due to its common shell composition (FeOOH). In this study, a much higher removal capacity of Pb(II) is observed (1667 mg Pb(II)/g Fe), which is over 100% higher than the highest removal capacity of nZVI reported before. High-resolution X-ray photoelectron spectroscopy (HR-XPS) reveals that through restricting the dehydration process of $Fe(OH)_3$, nZVI can acquire a unique shell, which is composed of 45.5% $Fe(OH)_3$ and 54.5% FeOOH. The presence of $Fe(OH)_3$ suppresses the reduction of Pb(II), but greatly promotes the co-precipitation and adsorption of Pb(II). Combining the ratio of Fe-released to Pb-immobilized and the result of HR-XPS, a reaction between Fe^0 core, $Fe(OH)_3$, and Pb(II) is proposed. The Fe released from the Fe^0 core leads to the core depletion, observed by transmission electron microscopy (TEM) under high Pb(II) loading. While temperature has little influence on the removal capacity, pH affects the removal capacity greatly. pH < 4.5 favors Fe dissolution, while pH > 4.5 promotes Pb(II) adsorption. Given the high Pb removal capacity via the $Fe(OH)_3$ shell, nZVI can be used to remedy Pb(II) contamination.

© 2013 Elsevier B.V. All rights reserved.

1. Introduction

Lead (Pb) is a hazardous heavy metal which can accumulate in the human body, causing damage to the brain, red blood cells and kidneys [1]. Its widespread presence in water has attracted close attention all over the world. In China, the total amount of lead in wastes from the lead-acid batteries industry adds up to 2000–2500 ton per year, contaminating a large amount of water. Hence, it is urgent to develop effective measures to treat the wastes. Conventional processes such as chemical precipitation, ion-exchange, membrane and reverse osmosis process are often employed [2–4]. However, these methods have been found to be limited due to the generation of secondary pollutants or poor removal efficiency. Adsorption is a promising process for Pb(II) removal because this technique is simple and efficient. Yet due to the high Pb(II) concentration in the wastewater from lead-acid batteries industry, the appropriate adsorbent needs to have high adsorption capacity. Recent studies have indicated that nZVI, an ideal adsorbent with strong reducing power, has many advantages with respect to treating waters polluted by heavy metals, such as high removal capacity and easy solid-liquid separation [5–11]. These inherent merits of nZVI make it perfect to remove Pb(II) from wastewater.

* Corresponding author at: State Key Laboratory of Pollution Control and Resources Reuse, Tongji University, Shanghai 200092, China. Tel.: +86 21 65982503; fax: +86 21 65988885.
** Corresponding author. Tel.: +86 21 65982503; fax: +86 21 65988885.
E-mail addresses: zhangyalei@tongji.edu.cn (Y. Zhang),
zhouxuefei@tongji.edu.cn (X. Zhou).

Employing nZVI to sequester Pb(II) in aqueous solution involves two processes, namely adsorption and reduction [6,12]. Previous studies have confirmed that the unique core–shell structure of nZVI imparts its strong reducing power and high adsorption capacity [13–15]. For metal cations with standard potential (E^0) more positive than that of iron, the removal mechanism is predominantly reduction; metals with E^0 slightly more positive such as Pb(II) can be immobilized at the nanoparticle surface by both reduction and adsorption, but mainly adsorption [6]. With regard to the adsorption, the shell of nZVI plays an important role in the immobilization process. nZVI reduced from borohydride is clad in a smooth amorphous oxide skin and FeOOH is considered as the main iron oxide phase of nZVI [5,6,16]. Besides functioning as a semiconductor for charge transport in the reduction process [17], the thin FeOOH layer provides the main bonding sites, hydroxyl groups, for heavy metal cations [18–20]. In other words, the quantity of surface hydroxyl groups determines the adsorption capacity of nZVI. Given that FeOOH is the dehydrated form of Fe(OH)$_3$ [6], it is possible to raise the number of hydroxyl groups by restricting the dehydration process of Fe(OH)$_3$ to improve the adsorption capacity of nZVI. Nonetheless, there is scant information in the literature on the implications of the Fe(OH)$_3$ shell, let alone the application of this kind of core–shell nanostructure.

The goal of this work is to explore the synergic effects of core–shell nanoparticles for immobilization of Pb(II). HR-XPS is applied to investigate the shell composition. In this study, pH and temperature effects on Pb(II) removal performance are studied as well. We believe that Pb(II) can serve as a model demonstrating the surface mechanisms of adsorption, co-precipitation, and reduction by nZVI particles with Fe(OH)$_3$ shell. The results from this study can be used to assess their utility for Pb(II) removal from heavy contaminated water.

2. Materials and methods

2.1. Chemical reagents

Analytic grade lead acetate (Pb[CH$_3$COO]$_2$·3H$_2$O), sodium borohydride (NaBH$_4$, 98%), ferric chloride anhydrous (FeCl$_3$) were purchased from Aladin (Shanghai, China), sodium acetate (CH$_3$COONa) and acetic acid (CH$_3$COOH) were obtained from Sinopharm Chemical Reagent Shanghai Co., Ltd (Shanghai, China). All chemicals were used without further purification.

2.2. nZVI synthesis methods

Based on the following reaction equation:

$$4Fe^{3+} + 3BH_4^- + 9H_2O \rightarrow 4Fe^0 + 3H_2BO_3^- + 6H_2 + 12H^+ \tag{1}$$
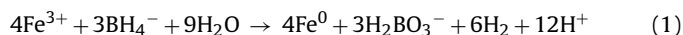
sodium borohydride (NaBH$_4$, 98%, 0.25 M) was introduced into anhydrous ferric chloride (FeCl$_3$, 0.048 M) through titration (titration rate 1 L/h) with a volume ratio of 1:1. After reduction, the jet-black iron nanoparticles were collected and washed with deionized (DI) water (>100 mL/g) and anhydrous ethanol three times respectively using a powerful magnet made of neodymium iron boron to separate solids and liquids instead of vacuum filtration [5–7]. Finally, fresh nZVI particles were stored in anhydrous ethanol solution instead of 5% ethanol solution [5–7] at 4 °C in order to avoid oxidization and dehydration.

2.3. TEM, XPS, and XRD analysis

High-resolution TEM with an energy dispersion spectrometer (Hitachi S-3000N) was performed using a JEOL JEM 2011 operated at 200 kV. Samples were prepared by depositing a few droplets of
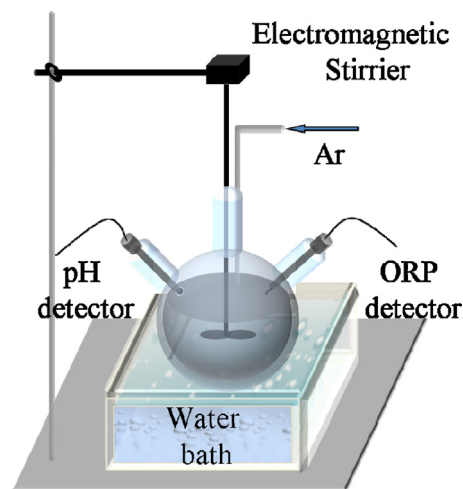

Fig. 1. Reactor for batch tests.

a dilute nZVI solution in 100% ethanol onto a carbon-coated TEM grid in an anaerobic chamber. The samples were briefly exposed to air during transfer from the anaerobic chamber to the microscope.

The XPS spectra were obtained by using a Perkin Elmer PHI 5000 ESCA System with Al Kα radiation at 1486.6 eV. The sample was first pressed to a 1 mm × 13 mm disk and fixed to the sample-holder in the pretreatment chamber; it was kept soaked in anhydrous ethanol to minimize the oxidation by air. After the alcohol was evaporated, the sample was transferred in situ to the test chamber for XPS study.

X-ray diffraction (XRD) was carried out on a Bruker D8 Advance X-ray diffraction instrument (Cu Kα) and the diffraction angle (2θ) from 10° to 90° was scanned.

2.4. Batch experiments

Batch experiments for Pb(II) adsorption were carried out in a 3-neck flask under Ar atmosphere. A 1000 mg/L Pb(CH$_3$COO)$_2$ stock solution was used for all experiments. The concentration range for Pb(II) was from 200 to 400 mg/L and the dose of iron nanoparticles was 250 mg/L. The flask was agitated vigorously by an electromagnetic stirrer (250 rpm) at 25 °C. During the first 30 min, aqueous sample was collected every 5 min while in following 45 min aqueous sample was collected every 15 min. Throughout the experiment, pH was monitored.

Tests of pH effect on Pb(II) removal were carried out in a series of 100 mL conical flasks sealed with screw caps. The concentration range for Pb(II) was from 400 to 1000 mg/L and the nZVI dose was 500 mg/L. The bottles were agitated vigorously on a shaker table (200 rpm) at 25 °C. Sodium acetate and acetic acid were used to adjust pH value to 3, 4, 5, and 6. After 90 min, aqueous sample was collected and analyzed.

To investigate the effect of temperature on adsorption, batch tests were performed at different temperatures (25, 30, 35 °C) in a series of 100 mL conical flasks sealed with screw caps. The initial Pb(II) concentrations were 200, 400, 600, and 800 mg/L and the nZVI dose was 500 mg/L. After 90 min, solution pH was measured, and aqueous samples were collected and analyzed.

Repetition of Pb(II) adsorption tests were carried out to verify the relationship between Fe-released and Pb-immobilized over time and different cycles. An aliquot of 8.5 mL (10 g Pb/L) lead acetate was spiked every 15 min from 0 min into a three-necked flask (in Fig. 1) containing 500 mL solution (nZVI, 2 g/L) under Ar atmosphere. In this case, the oxidation-reduction potential (ORP) and pH were monitored continuously (HACH Sc200, America), and
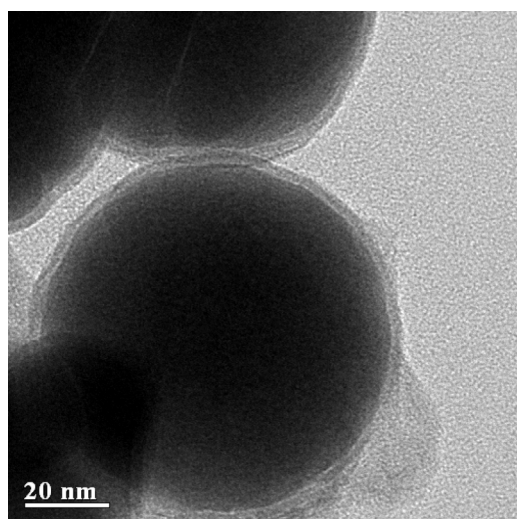
Fig. 2. TEM micrograph of the fresh nZVI.

samples were collected every 10 min until 200 min, then every 20 min to the end.

Lead and iron cations in all collected samples were determined by inductively coupled plasma (ICP, Agilent 720ES, Japan) after filtering with 0.22 μm filter and acidifying with 4% ultrahigh purity HNO₃. The final solid was kept in anhydrous ethanol until TEM and XPS analysis. All tests were performed in triplicate; analysis of variance (ANOVA) was used to test the significance of results and $p < 0.05$ was considered to be statistically significant.

3. Results and discussion

3.1. Characterization of the synthesized nZVI

The microstructure of synthesized nZVI was carefully examined by HR-TEM. The representative single particle size distribution was around 50–70 nm, as illustrated in Fig. 2. Examinations of a number of particles with sizes from 10 to 200 nm showed that all particles had similar surface layers, which resulted from the oxidation and reaction with oxygen and water. It verifies that nZVI has specific core–shell structure, a core of zero-valent iron and a thin shell of iron oxides [21,22]. The XRD pattern (Fig. 3) of nZVI also suggested that Fe was mainly in its Fe^0 state (characterized by the basic reflection appearing at a 2θ value of 44.7–44.8°). However, the Fe^0 core
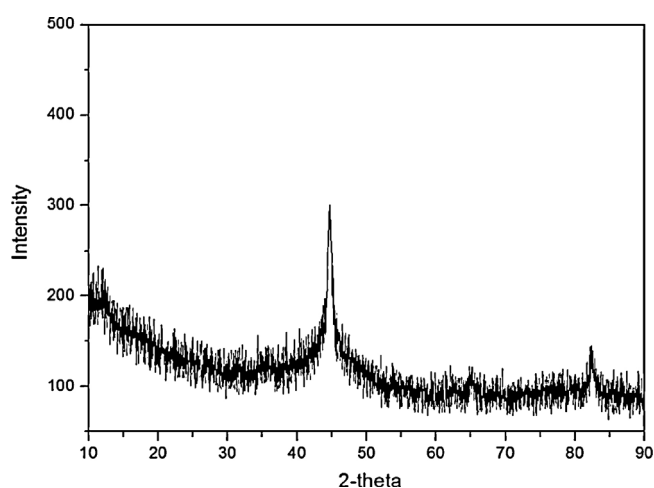

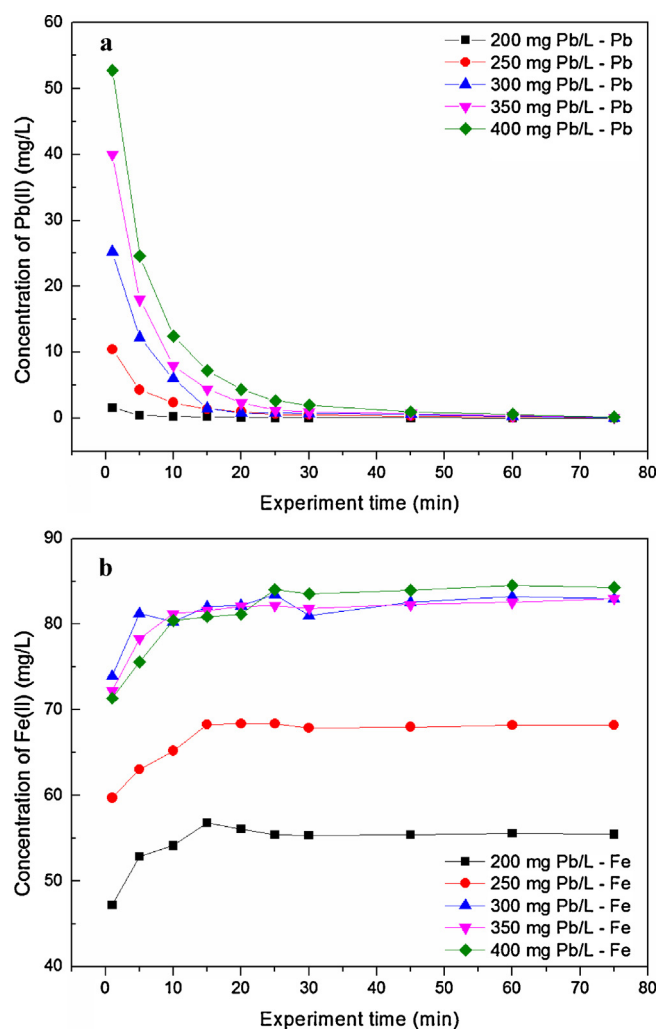**Fig. 3.** XRD pattern of the fresh nZVI.

Fig. 4. (a) Trends of Pb(II) concentrations during the experiment with initial Pb(II) concentration of 200, 250, 300, 350, and 400 mg/L (250 mg/L, nZVI); (b) Trends of Fe(II) concentrations during the experiment with initial Pb(II) concentration of 200, 250, 300, 350, and 400 mg/L (250 mg/L, nZVI).

did not give rise to a highly crystalline *bcc* iron phase and iron oxides were also not detected, which may be due to the high degree of disorder. This result is in line with the universal acknowledgment that the fresh nZVI with high reductive and adsorptive activity has a low crystallinity of the metal phase and highly disordered iron oxides [23].

3.2. Pb(II) sequestration performance of nZVI

Fig. 4 illustrates the trends in Pb(II) and Fe(II) concentrations over time during the adsorption tests. Dosing with 250 mg/L nZVI particles resulted in a rapid decrease of Pb(II) concentrations and a corresponding rise of Fe(II) concentration. When the initial Pb(II) concentration was lower than 300 mg/L, higher Fe(II) concentration correlated well with higher Pb(II) concentration. Moreover, the mole ratio of Fe-released to Pb-immobilized was very close to 1. However, when the initial Pb(II) concentration went from 300 to 400 mg/L, there was no evident increase in Fe(II) concentration detected. It was not surprising that an initial high Pb removal rate was observed, but the high Fe(II) concentration was unexpected. From 0 to 30 min, the concentration of Pb(II) decreased slowly and Fe(II) increased gradually. At the end of 75 min no Pb(II) was detected and Fe(II) concentration remained almost the same as it was at 30 min. Additionally, the solution pH values in these
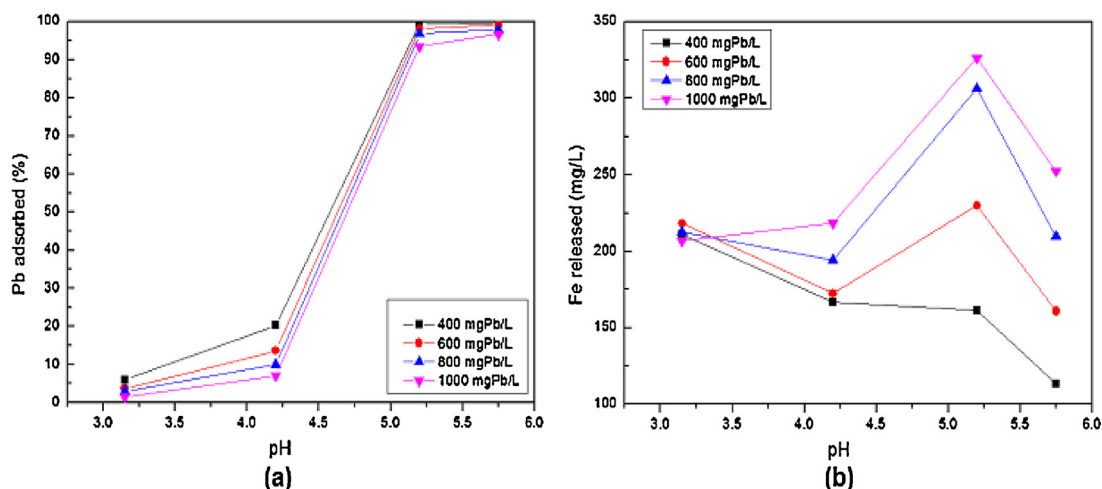
Fig. 5. (a) Pb(II) removal rate at different pH values (3, 4, 5, and 6) (initial Pb(II) concentration: 400, 600, 800, and 1000 mg/L; nZVI, 500 mg/L); (b) final Fe concentration in solution under different pH values (3, 4, 5, and 6) (initial Pb(II) concentration: 400, 600, 800, and 1000 mg/L; nZVI, 500 mg/L).

experiments ranged between 5.5 and 6.5 (data not shown), which was below the precipitation point of 7.1 for a Pb(II) concentration of 1000 mg/L, calculated from the solubility product constant provided by Pauling [24]. Hence, the conventional Pb(II) precipitation (reaction 2) has little influence on Pb(II) removal performance.

$$Pb^{2+} + 2H_2O \rightarrow Pb(OH)_2\downarrow + 2H^+ \qquad (2)$$

To better understand the kinetics of the adsorption process, a pseudo second-order model was applied [25]. Table A1 presents the results of model fit, with a correlation coefficient (r^2) of 1. Based on the pseudo second-order model, the adsorbate and adsorbent share electrons during the adsorption process [25].

3.3. Effect of pH on Pb(II) sequestration

pH is an important factor for Pb(II) sequestration by nZVI. It is widely accepted that low pH has a negative effect on metal adsorption by nZVI. When pH is lower than the isoelectric point of nZVI, the positive charge surface will repulse metal cations [6]. Moreover, Fe^0 will dissolve very rapidly at low pH [26]. However, there is limited information in the literature regarding the exact pH value at which Pb(II) adsorption will be totally inhibited. Fig. 5 presents the results from batch experiments in which iron nanoparticles are exposed to lead acetate solution with different pH values. Pb(II) removal rate > 99% when pH is above 5.0 while almost no Pb(II) is removed at pH ~3 (Fig. 5a); Fe dissolution is a dominant process when pH value is below 4 taking consideration of the high Fe(II) concentration (Fig. 5b) and low Pb(II) removal rate. Combining Fig. 5a and b, one can conclude that pH < 4.5 favors Fe dissolution while pH > 4.5 promotes metal adsorption. Since Fe dissolution diminishes as pH increases, the increase in Fe(II) concentration as pH increases from 4 to 5 is caused by Pb sequestration. Additionally, the removal capacity of nZVI for Pb(II) is higher than 1600 mg/g, which is much higher than that of other adsorbents, such as poly-elemental mesoporous adsorbent (367 mg/g) [27] and carbon nanotubes with surface-bound humic acid (250 mg/g) [28].

3.4. Effect of temperature on Pb(II) adsorption

Temperature is another factor that can influence adsorption capacity. An increase in temperature resulted in gradual increase of Pb(II) adsorption capacity (Fig. 6). In Fig. 6, it is interesting to note that the concentration of Fe-released is almost equal to the theoretical Fe concentration (calculated from reaction (11)). In

addition, solution pH values in these tests were all below the precipitation point of 7.1 (mainly between 5.5 and 6.0), which meant conventional Pb(II) precipitation was not going to occur. To better understand the adsorption of Pb(II) cations by nZVI, the Freundlich isotherm was used to fit the data (Table A2), with high r^2 [24]. The adsorption isotherm is classical L-type isotherm, an indication of chemisorption, reflecting a high affinity between Pb(II) and nZVI; the adsorption process is endothermic.

3.5. TEM analysis on the core–shell structure of nZVI

To investigate the microstructure of the residual solid after adsorption directly, TEM with an energy dispersion spectrometer was used. Fig. 7a and b shows TEM images of nZVI that has reacted with low and high concentration of Pb(II) respectively. The core–shell structure remained largely unaltered under low Pb(II) concentration (Fig. 7a) and Pb(II) cations adhered to the surface of nZVI particles suggested by the result of EDS analysis (Fig. 7c). However, in Fig. 7b, the Fe(0) core in a fraction of the nanoparticles was depleted, leaving behind empty iron oxide shells. This indicates
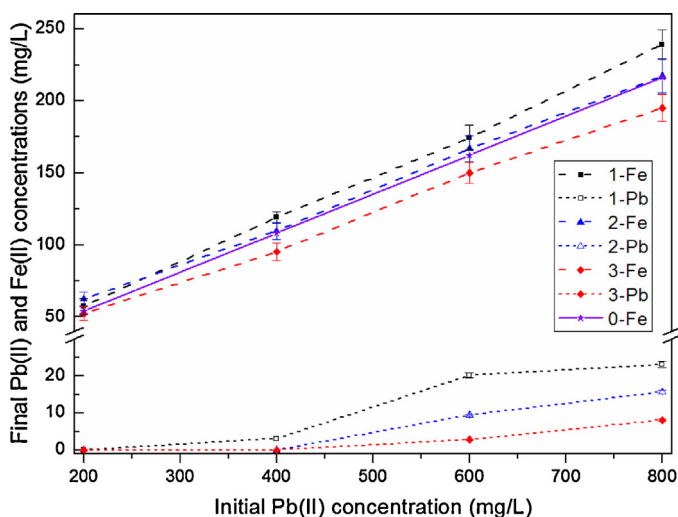

Fig. 6. Final concentration of Pb(II) and Fe(II) under different initial Pb(II) concentrations and different temperatures. Pb(II) concentration: 200, 400, 600, and 800 mg/L; nZVI concentration: 500 mg/L; temperature: test 1, 2, and 3, 25 °C, 30 °C, and 35 °C; 0-Fe represents the theoretical concentration of Fe if the ratio of Fe-released to Pb-adsorbed is 1 (see reaction (11)).
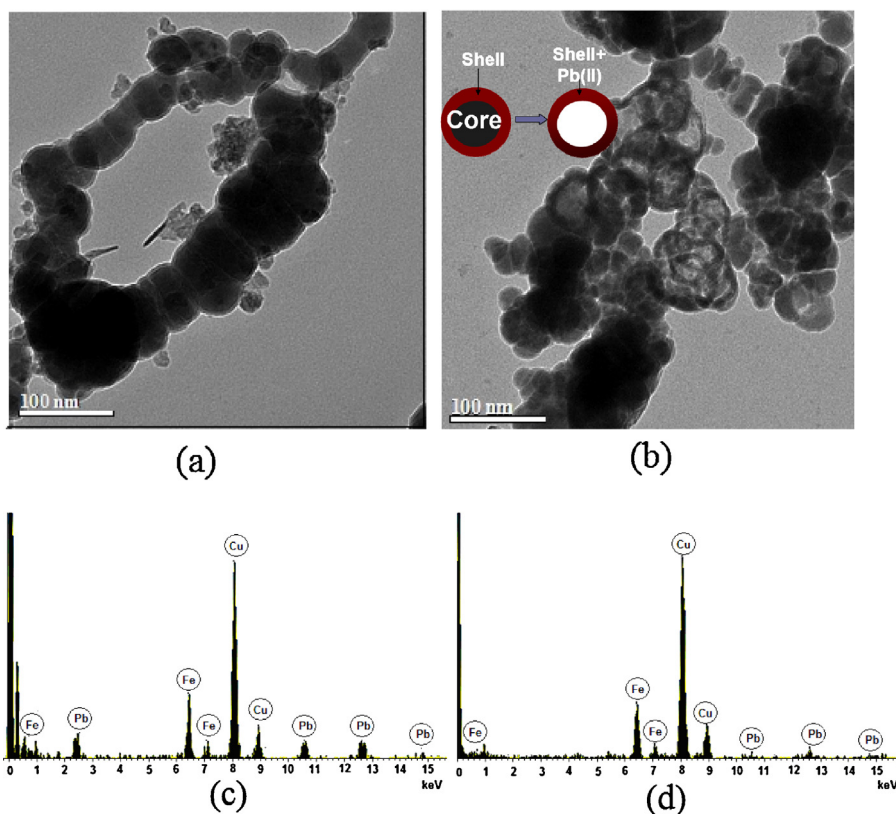
Fig. 7. (a) TEM image of nZVI (500 mg/L) reacted with low concentration of Pb(II) (200 mg/L) for 2 h; (b) TEM image of nZVI (500 mg/L) reacted with high concentration of Pb(II) (800 mg/L) for 2 h; (c) EDS spectrum of solid adhering to nZVI; (d) EDS spectrum of empty iron oxide shell.

that the nanoparticles shell is able to facilitate charge flow [23] and Fe(II) cations in solution come from the Fe(0) core. Through EDS analysis, it was observed that a small fraction of Pb(II) entered into iron oxide shell (Fig. 7d). The appearance of empty iron oxide shells correlates with increasing Pb(II) concentration.

3.6. Core–shell structure of nZVI

Fig. 8a is an Fe 2p XPS survey scan of the iron nanoparticles (250 mg/L) before and after exposure to 500 mg/L Pb(II). The photoelectron peaks at 711, 720 and 725 eV represent the binding energies of 2p3/2, shake-up satellite 2p3/2 and 2p1/2, respectively [5], indicating the existence of a layer of iron oxides [29]. Furthermore, a small peak at 706.5 eV suggests that zero-valent iron is also present. The coexistence of a large fraction of iron oxides and a relatively small amount of ZVI confirms the core–shell structure of nZVI.

Previous studies indicated that FeOOH was the main component of the nZVI shell [5,6]. However, in this study, a distinct difference was identified. It is hard to discern iron oxide speciation only from the Fe 2p region spectrum, since both $Fe(OH)_3$ and FeOOH have similar peak positions in this region. Hence, O 1s survey scan was further conducted to delineate the surface oxygen states and identify Fe states (Fig. 8b). The O 1s region can be decomposed into three peaks at 529.6, 531.0 and 532.2 eV, corresponding to O^{2-}, —OH and chemically or physically adsorbed water, respectively. Since the ratio of OH to O^{2-} on the surface was approximately 3.5 (Table 1), it is reasonable to conclude that the shell was composed of 45.5% $Fe(OH)_3$ and 54.5% FeOOH. The different chemical constituents of the nZVI shell are likely due to the following two factors. The first one is the relatively high concentration of sodium borohydride. During synthesis process, the side reaction between sodium borohydride and water produces hydrogen which could

prevent the oxidation of Fe(0). The other one is the different storage conditions, since in this study the freshly prepared nZVI was stored in 100% ethanol while in other studies nZVI was kept in 5% ethanol [5,6]. The presence of H_2O in the storage environment may facilitate the transformation from $Fe(OH)_3$ to FeOOH. With regard to Pb(II) adsorption, $Fe(OH)_3$ has two more binding sites for Pb(II) than FeOOH. Indeed, the Pb(II) removal capacity of nZVI in this study is much higher than other studies [5,6,30]. Hence, there is a substantial improvement in the Pb(II) removal capacity of nZVI with $Fe(OH)_3$ shell.

After Pb(II) exposure, there are some obvious changes within the "shell". Some peak broadening at ~708.5 eV suggests the appearance of a new Fe(II) component in the "shell" [31]. Combined with the decrease of Fe(III) on the surface, a likely explanation for the increasing Fe(II) content is that $Fe(OH)_3$ is reduced to $Fe(OH)_2$ by zerovalent iron (ZVI). In addition, it is noted that the ratio of detected ZVI increases in the later period of the adsorption (from 90 min to 360 min) (Table 1). Considering the depth that XPS can reach remains the same, it is likely that the thickness of the shell decreases as adsorption of Pb(II) progresses. It is possible that the structure of derived $Fe(OH)_2$ is compacter than that of native $Fe(OH)_3$.

3.7. Interactions among metallic iron, $Fe(OH)_3$, and Pb(II) ions

In terms of Pb(II) reduction, only a small part of Pb(II) was reduced to Pb(0) (~136.6 eV) and almost over 90% of Pb existed as Pb(II) (Pb-O, ~138.2 eV) on the surface of nZVI particles (Fig. 8c, Table 1). While at first it was unexpected that Pb(II) ($E^0 = -0.12$ V) was not reduced, once the $Fe(OH)_3$ shell is considered, it is clear that it is more prone to be reduced [32].

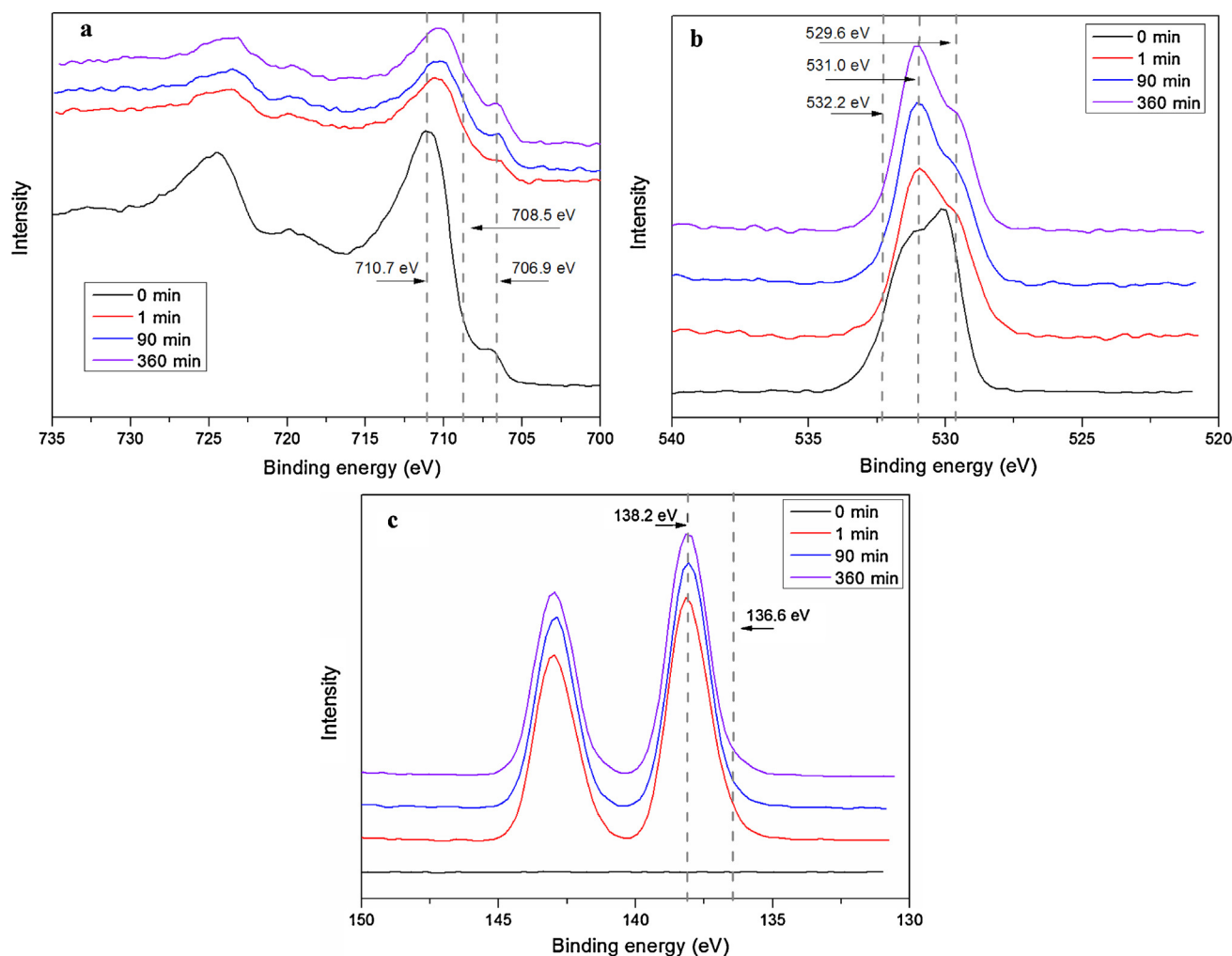$$Fe(OH)_3\,(s) + H^+ + e^- \rightarrow Fe(OH)_2\,(s) + H_2O \qquad (3)$$
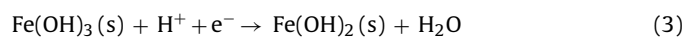
Fig. 8. XPS spectra of the fresh nZVI and nZVI (250 mg/L) reacting with 500 mg/L Pb(II) after 1 min, 90 min, and 360 min. (a) Iron HR-XPS spectra in fresh nZVI and nZVI after reaction; (b) oxygen HR-XPS spectra in fresh nZVI and nZVI after reaction; (c) lead HR-XPS spectra in fresh nZVI and nZVI after reaction. (For interpretation of the references to color in this figure legend, the reader is referred to the web version of the article.)

As the initial pH was below 6, the calculated E^0 for $Fe(OH)_3$ was higher than -0.1 V considering:

$$E^0 = p\varepsilon(2.3\,RTF^{-1}) = 0.059 \times (4.3 - \text{pH}) > -0.1 \quad \text{(for Eq. (3))} \tag{4}$$

where $p\varepsilon$: electron activity at equilibrium; R: universal gas constant; T: temperature; F: Faraday; which was more positive than that of Pb(II). $Fe(OH)_3$ therefore would be reduced to $Fe(OH)_2$ (Eq. (3)) by zero-valent iron (ZVI) prior to Pb(II) reduction:

$$Pb^{2+} + 2e^- \rightarrow Pb \qquad E^0 = -0.12\,V \tag{5}$$
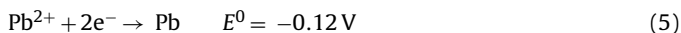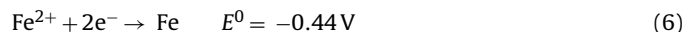
However, an FeOOH shell does exist, which can serve as the charge transport channel for Pb(II) reduction.

In batch tests, it was interesting to note that as soon as nZVI was added into Pb(II) solution, a certain amount of iron cations were released. Or rather, the ratio of Fe(II) released to Pb(II) immobilized was 1:1 when the initial concentration of Pb(II) was below 300 mg/L. In previous investigations [9,12,33], an initial high removal rate of heavy metal was observed. However, the mechanism behind this phenomenon has long been regarded as a physical property (i.e., that involves occlusion of nZVI) rather than a chemical process. In this study, not only were proportional iron cations detected, but also XPS showed Fe(III) was reduced to Fe(II) rapidly.

Table 1
Ratios of different components suggested by the result of XPS analysis of the fresh nZVI (0 min) and nZVI (250 mg/L) reacting with 500 mg/L Pb(II) after 1 min, 90 min, and 360 min.

| Time (min)	O (%)			Fe (%)			Pb (%)	
	O^{2-} (529.6 eV)	OH^- (531 eV)	H_2O (532.2 eV)	Fe^{3+} (710.7 eV)	Fe^{2+} (708.5 eV)	Fe^0 (706.5 eV)	PbO (138.2 eV)	Pb^0 (136.6 eV)
0	20	69.7	10.3	98	–	2	–	–
1	40.2	50.4	9.4	81.9	12.7	5.4	91.3	8.7
90	38.6	53.4	8	77.3	13.6	9.1	91.6	8.4
360	38.1	53.9	8	70.7	15.2	14.1	90.4	9.6

We would like to propose a chemical mechanism for the phenomenon of the initial high removal rate. There are seven possible reactions when nZVI is added into lead acetate solution (Eqs. (3), (5)–(9)) [32]:

$$Fe^{2+} + 2e^- \rightarrow Fe \qquad E^0 = -0.44\,V \tag{6}$$

$$Pb(Ac)_2 \rightarrow Pb^{2+} + 2Ac^- \tag{7}$$

$$Fe^{2+} + H_2O \rightarrow FeOH^+ + H^+ \tag{8}$$

$$Pb^{2+} + FeOH^+ \rightarrow PbOH^+ + Fe^{2+} \tag{9}$$

$$PbOH^+ + H_2O \rightarrow Pb(OH)_2 + H^+ \tag{10}$$

Reaction (9) is the crucial step and if this process is spontaneous, then reaction (7) will be largely accelerated because of the shift of chemical equilibrium. The net effect of these reactions is:

$$2Fe(OH)_3\,(s) + Fe + Pb(Ac)_2$$
$$\rightarrow Pb(OH)_2 + 2Fe(OH)_2\,(s) + 2Ac^- + Fe^{2+} \tag{11}$$
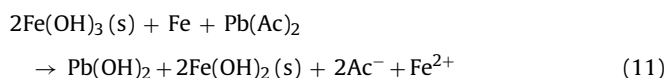
To explain the spontaneous reaction (9), two half-reactions, Eq. (8) and Eq. (12), are needed.

$$Pb^{2+} + H_2O \rightarrow PbOH^+ + H^+ \tag{12}$$
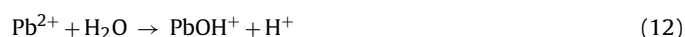
The Gibbs free energy of reaction (9) can be calculated from:

$$\Delta G_8 = -RT \ln \left[\frac{[PbOH^+] \cdot [Fe^{2+}]}{[FeOH^+] \cdot [Pb^{2+}]} \right] \tag{13}$$

where ΔG_8: the Gibbs free energy; $[PbOH^+]$, $[FeOH^+]$, $[Pb^{2+}]$, and $[Fe^{2+}]$: the concentration of $PbOH^+$, $FeOH^+$, Pb^{2+}, and Fe^{2+}. Eq. (13) can be formulated as follows:

$$\Delta G_8 = -RT \ln \left[\frac{[PbOH^+] \cdot [H^+]}{[Pb^{2+}]} \frac{[Fe^{2+}]}{[FeOH^+] \cdot [H^+]} \right]$$
$$= -RT \ln \left[\frac{K_{11}}{K_7} \right] < 0 \tag{14}$$

where K_7 and K_{11}: the equilibrium constants of reactions (8) and (12), which are well known [32]:

$$\log K_7 = \log \left[\frac{[FeOH^+] \cdot [H^+]}{[Fe^{2+}]} \right] = -9.5 \tag{15}$$

$$\log K_{11} = \log \left[\frac{[PbOH^+] \cdot [H^+]}{[Pb^{2+}]} \right] = -7.77 \tag{16}$$

Thus, the Gibbs free energy calculated from Eq. (14) for reaction (9) is less than 0. Hence, reaction (9) is a spontaneous reaction and it is reasonable to propose Eq. (11) to formulate the chemical processes that occur when nZVI is added into a Pb(II) solution. Reaction (11) is not only restricted by Pb(II) concentration, but also by the amount of Fe(OH)$_3$. This may explain why the initial Fe(II) concentration did not increase when Pb(II) was over 300 mg/L in Pb(II) adsorption experiment; it was Fe(OH)$_3$ limited. Moreover, seen from reaction (11), the iron cations released in solution come from the nZVI core. This logical deduction is corroborated by the result of TEM and XPS analysis. In TEM analysis, the hollow sphere indicates the depletion of Fe^0 core; in XPS analysis, the ratio of Fe(II, III)/Fe(0) before (0 min) and after Pb(II) (1 min) exposure remains the same. As soon as Pb(II) precipitates, Pb(OH)$_2$ will bond with Fe(OH)$_2$ and/or Fe(OH)$_3$ forming an Fe—O—Pb structure, which can be corroborated by XPS as a decrease in —OH and an increase in O^{2-}.
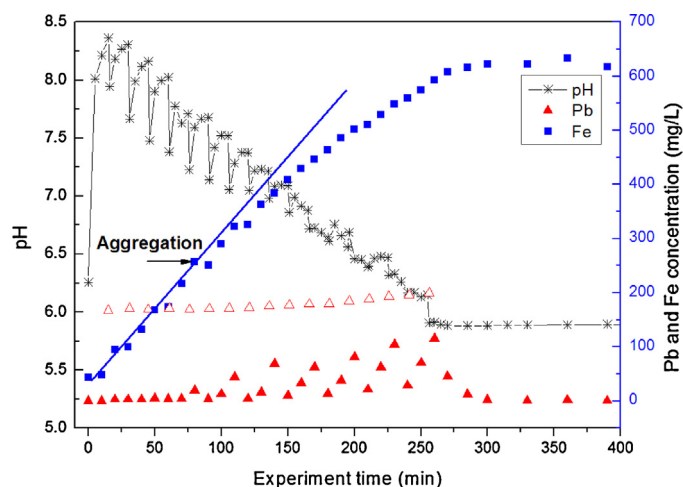

Fig. 9. Results of repetitive adsorption tests for corroborating that detected Fe(II) concentration could be predicted by reaction (11). nZVI concentration: 2 g/L; Blue line: theoretical value of released Fe(II) according to Eq. (11); ■: actual Fe(II) concentration in solution; △: theoretical value of Pb(II) concentration after every dose (total 18 times, every dose will make Pb(II) concentration in solution arrive at 200 mg/L); ▲: actual Pb(II) concentration in solution; *: actual pH in solution. (For interpretation of the references to color in this figure legend, the reader is referred to the web version of the article.)

To verify Eq. (11), repetitive Pb(II) adsorption tests were performed, where 8.5 mL (10 g Pb/L) lead acetate were spiked repeatedly every 15 min from 0 min onward into a three-necked flask containing 500 mL solution (nZVI, 2 g/L). The results are presented in Fig. 9. During the first 6 doses, as soon as Pb(II) was introduced, it was adsorbed immediately and Fe(II) was proportionally released into solution. Although the solution was weakly basic, E^0 of Fe(OH)$_3$ was still more positive than that of Fe(0) according to reaction (4). In addition, E^0 of Pb(II) in basic conditions was more negative than −0.5 V [34]. Therefore, Eq. (11) was still applicable in basic conditions. However, from the 7th dose and onward, the quantity of released Fe(II) was less than the theoretical value. The rising ORP curve (from initial −700 mV to final −500 mV, data not shown) suggested the aggregation of nZVI [35]. It was likely that the aggregation of nZVI caused by acetate adsorption-bridging, made it more difficult for electrons to transport from Fe(0) to Fe(OH)$_3$ which had formerly been facilitated by Pb(II) cations. Since the isoelectric point of nZVI was in the range of pH 8.1–8.3 [16], the surface of nanoparticles was positively charged in this experiment. Therefore, acetate was inclined to adsorb onto nanoparticles by electrostatic force, performing its adsorption-bridging effect. In addition, the Pb(II) removal capacity of nZVI in the repetitive study was also higher than 1600 mg/g and intermittent dosing did not affect the capacity significantly.

3.8. Implications for Pb(II) remediation

Previous studies of reactions between iron materials and Pb(II) focused chiefly on adsorption, co-precipitation and reduction processes induced by the shell or core of nZVI separately [6,7,30]. The dynamic reactions between core and shell of nZVI reported here suggest the composition of the shell has a crucial influence on Pb(II) removal mechanisms. Several previous studies have investigated the sequestration mechanism of metal cations by nZVI covered with a thin layer of FeOOH [6,7,30]. Given the chemical stability of FeOOH, an interaction between Fe^0 and FeOOH will not occur. However, in this study, Fe(OH)$_3$ is also the main component of the shell. It can be reduced by ZVI and consequently arrest charge transport. Thus, Fe(OH)$_3$ suppresses the reduction of Pb(II). Nevertheless, this process will contribute to Pb(II) adsorption
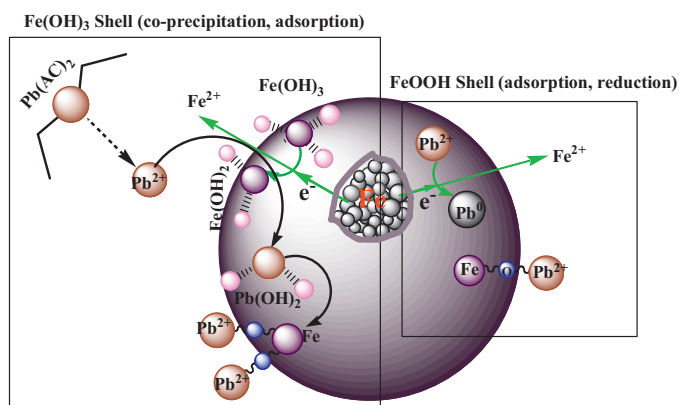
Fe(OH)$_3$ Shell (co-precipitation, adsorption)

Fig. 10. Conceptual model for the reaction between Pb(CH$_3$COO)$_2$ and nZVI.

and co-precipitation. A conceptual model (Fig. 10) is constructed to facilitate the understanding on experimental results. According to reaction (11), proportional Pb(II) precipitates out of solution when Fe(OH)$_3$ is reduced. Moreover, there are many more surface hydroxyl groups from Fe(OH)$_3$. This provides many binding sites for Pb(II) adsorption, so the Pb(II) removal capacity of the nZVI in this study is over 100% higher than the highest removal capacity (813 mg Pb/g Fe) of nZVI reported before [29]. In conclusion, Fe(OH)$_3$ promotes the co-precipitation and adsorption of Pb(II) while inhibiting the reduction. It is worth sacrificing some reducing capacity for higher adsorption capacity.

4. Conclusions

In this study, the dehydration process of Fe(OH)$_3$ was restricted to synthesize a novel nZVI core–shell structure. nZVI with a shell of 45.5% Fe(OH)$_3$ and 54.5% FeOOH exhibited a high efficacy for removing Pb(II) from liquid solution. On the basis of the results, the following conclusions can be drawn:

(1) Pb(II) removal capacity using this nZVI is 1667 mg Pb(II)/g Fe, which is over 100% higher than the highest removal capacity of other nZVI reported before.
(2) The presence of Fe(OH)$_3$ suppresses the reduction of Pb(II), but greatly promotes the co-precipitation and adsorption of Pb(II). Combining the ratio of Fe-released to Pb-immobilized and the result of HR-XPS, a specific reaction between Fe^0 core, Fe(OH)$_3$ and Pb(II) is proposed.
(3) Fe released from the Fe^0 core leads to core depletion (observed by TEM under high Pb(II) loading).
(4) While temperature has little influence on the removal capacity, pH affects the removal capacity significantly. pH < 4.5 favors Fe dissolution, while pH > 4.5 promotes Pb(II) adsorption.

Acknowledgements

Appendix A. Supplementary data

Supplementary data associated with this article can be found, in the online version, at http://dx.doi.org/10.1016/j.jhazmat.2013.10.031.

References

[1] H. Needleman, Lead poisoning, Annu. Rev. Med. 55 (2004) 209–222.
[2] Q. Chen, Z. Luo, C. Hills, G. Xue, M. Tyrer, Precipitation of heavy metals from wastewater using simulated flue gas: sequent additions of fly ash, lime and carbon dioxide, Water Res. 43 (2009) 2605–2614.
[3] S. Malamis, E. Katsou, K.J. Haralambous, Study of Ni(II), Cu(II), Pb(II), and Zn(II) removal using sludge and minerals followed by MF/UF, Water Air Soil Pollut. 218 (1–4) (2011) 81–92.
[4] L. Wang, L. Yang, Y. Li, Y. Zhang, X. Ma, Z. Ye, Study on adsorption mechanism of Pb(II) and Cu(II) in aqueous solution using PS-EDTA resin, Chem. Eng. J. 163 (2010) 364–372.
[5] X.Q. Li, W.X. Zhang, Iron nanoparticles: the core–shell structure and unique properties for Ni(II) sequestration, Langmuir 22 (2006) 4638–4642.
[6] X.Q. Li, W.X. Zhang, Sequestration of metal cations with zero valent iron nanoparticles—a study with high resolution X-ray photoelectron spectroscopy (HR-XPS), J. Phys. Chem. C 111 (2007) 6939–6946.
[7] M.A.V. Ramos, W.L. Yan, X.Q. Li, B.E. Koel, W.X. Zhang, Simultaneous oxidation and reduction of arsenic by zero-valent iron nanoparticles: understanding the significance of the core shell structure, J. Phys. Chem. C 113 (2009) 14591–14594.
[8] W.L. Yan, M.A.V. Ramos, B.E. Koel, W.X. Zhang, As(III) sequestration by iron nanoparticles: study of solid-phase redox transformations with X-ray photoelectron spectroscopy, J. Phys. Chem. C 116 (2012) 5303–5311.
[9] S. Klimkova, M. Cernik, L. Lacinova, J. Filip, D. Jancik, R. Zboril, Zero-valent iron nanoparticles in treatment of acid mine water from in situ uranium leaching, Chemosphere 82 (2011) 1178–1184.
[10] G. Lopez-Tellez, C.E. Barrera-Diaz, P. Balderas-Hernandez, G. Roa-Morales, B. Bilyeu, Removal of hexavalent chromium in aquatic solutions by iron nanoparticles embedded in orange peel pith, Chem. Eng. J. 173 (2011) 480–485.
[11] M. Gheju, Hexavalent chromium reduction with zero-valent iron (ZVI) in aquatic systems, Water Air Soil Pollut. 222 (2011) 103–148.
[12] S. Ponder, J. Darab, T. Mallouk, Remediation of Cr(VI) and Pb(II) aqueous solutions using supported nanoscale zero-valent iron, Environ. Sci. Technol. 34 (2000) 2564–2569.
[13] W.L. Yan, A. Herzing, X.Q. Li, C.J. Kiely, W.X. Zhang, Structural evolution of Pd-doped nanoscale zero-valent iron (nZVI) in aqueous media and implications for particle aging and reactivity, Environ. Sci. Technol. 44 (2010) 4288–4294.
[14] J.T. Nurmi, P.G. Tratnyek, V. Sarathy, D.R. Baer, J.E. Amonette, K. Pecher, C. Wang, J.C. Linehan, D.W. Matson, R.L. Penn, M.D. Driessen, Characterization and properties of metallic iron nanoparticles: spectroscopy, electrochemistry, and kinetics, Environ. Sci. Technol. 39 (2005) 1221–1230.
[15] Y. Liu, S.A. Majetich, R.D. Tilton, D.S. Sholl, G.V. Lowry, TCE dechlorination rates, pathways, and efficiency of nanoscale iron particles with different properties, Environ. Sci. Technol. 39 (2005) 1338–1345.
[16] Y.P. Sun, X.Q. Li, J.S. Cao, W.X. Zhang, H.P. Wang, Characterization of zero-valent iron nanoparticles, Adv. Colloid Interface Sci. 120 (2006) 47–56.
[17] C.M. Wang, D.R. Baer, J.E. Amonette, M.H. Engelhard, J. Antony, Y. Qiang, Morphology and oxide shell structure of iron nanoparticles grown by sputter-gas-aggregation, Nanotechnology 18 (2007) 255603, 7 pp.
[18] H. Abdel-Samad, P.R. Watson, An XPS study of the adsorption of lead on goethite (α-FeOOH), Appl. Surf. Sci. 136 (1998) 46–54.
[19] B.A. Manning, J.R. Kiser, H. Kwon, S.R. Kanel, Spectroscopic investigation of Cr(III)-and Cr(VI)-treated nanoscale zerovalent iron, Environ. Sci. Technol. 41 (2007) 586–592.
[20] S.R. Kanel, B. Manning, L. Charlet, H. Choi, Removal of arsenic(III) from ground water by nanoscale zero-valent iron, Environ. Sci. Technol. 39 (2005) 1291–1298.
[21] K. Sohn, S.W. Kang, S. Ahn, M. Woo, S.K. Yang, Fe(0) nanoparticles for nitrate reduction: stability, reactivity, and transformation, Environ. Sci. Technol. 40 (2006) 5514–5519.
[22] B.I. Kharisov, H.V. RasikaDias, O.V. Kharissova, V.M. Jimenez-Perez, B.O. Perez, B.M. Flores, Iron-containing nanomaterials: synthesis, properties, and environmental applications, RSC Adv. 2 (2012) 9325–9358.
[23] W.L. Yan, H.L. Lien, B.E. Koel, W.X. Zhang, Iron nanoparticles for environmental clean-up: recent developments and future outlook, Environ. Sci.: Process Impacts. 15 (2013) 63–77.
[24] L. Pauling, General Chemistry, 3rd ed., Dover Publications, San Francisco, 1970.
[25] P. Xu, G.M. Zeng, D.L. Huang, C. Lai, M.H. Zhao, Z. Wei, N.J. Li, C. Huang, G.X. Xie, Adsorption of Pb(II) by iron oxide nanoparticles immobilized *Phanerochaete chrysosporium*: equilibrium, kinetic, thermodynamic and mechanisms analysis, Chem. Eng. J. 203 (2012) 423–431.
[26] R.T. Wilkin, M.S. McNeil, Laboratory evaluation of zero-valent iron to treat water impacted by acid mine drainage, Chemosphere 53 (7) (2003) 715–725.
[27] X.W. Wu, H.W. Ma, J. Yang, F.J. Wang, Z.H. Li, Adsorption of Pb(II) from aqueous solution by a poly-elemental mesoporous adsorbent, Appl. Surf. Sci. 258 (2012) 5516–5521.
[28] D.H. Lin, X.L. Tian, T.T. Li, Z.Y. Zhang, X. He, B.S. Xing, Surface-bound humic acid increased Pb^{2+} sorption on carbon nanotubes, Environ. Pollut. 167 (2012) 138–147.
[29] A.P. Grosvenor, B.A. Kobe, M.C. Biesinger, N.S. McIntyre, Investigation of multiplet splitting of Fe 2p XPS spectra and bonding in iron compound, Surf. Interface Anal. 36 (2004) 1564–1574.

[30] Y.F. Xi, M. Mallavarapu, R. Naidu, Reduction and adsorption of Pb^{2+} in aqueous solution by nano-zero-valent iron-a SEM, TEM and XPS study, Mater. Res. Bull. 45 (2010) 1361–1367.

[31] D.R. Baer, D.J. Gaspar, P. Nachimuthu, S.D. Techane, D.G. Castner, Application of surface chemical analysis tools for characterization of nanoparticles, Anal. Bioanal. Chem. 396 (2010) 983–1002.

[32] W. Stumm, J.J. Morgan, Aquatic Chemistry, 3rd ed., Wiley & Sons, New York, 1996.

[33] A. Alqudami, N.A. Alhemiary, S. Munassar, Removal of Pb(II) and Cd(II) ions from water by Fe and Ag nanoparticles prepared using electro-exploding wire technique, Environ. Sci. Pollut. Res. 19 (2012) 2832–2841.

[34] R.C. Weast, Handbook of Chemistry and Physics, 70th ed., CSC press, Boca Raton, FL, 1989–1990.

[35] Z.Q. Shi, J.T. Nurmi, P.G. Tratnyek, Effects of nano zero-valent iron on oxidation–reduction potential, Environ. Sci. Technol. 45 (2011) 1586–1592.